Calorimetric examination of suitability of calcium, cobalt and nickel nitrate hydrates for thermal energy storage

P. Honcová[1*], G. Sádovská[1,2], L. Binder[1], P. Koštál[1], D. Honc[3]

[1]Faculty of Chemical Technology, University of Pardubice, Doubravice 41, 53210 Pardubice, Czech Republic

[2]J. Heyrovský Institute of Physical Chemistry, Academy of Science of the Czech Republic, Dolejskova 3, 182 23 Praha 8, Czech Republic

[3]Faculty of Electrical Engineering and Informatics, University of Pardubice, Cs. Legii Sq. 565, 53002 Pardubice, Czech Republic

DOI 10.1007/s10973-020-09435-y

Abstract

Selected nitrate hydrates were characterized using X-ray diffraction, helium pycnometer, Calvet type calorimeter and simultaneous termogravimeter coupled with differential scanning calorimeter. Melting and crystallization of all studied nitrate hydrates were observed by differential scanning calorimeter, and the supercooling (difference between melting temperature and crystallization temperature) was found to be more than 80, 14 and 37 °C for calcium nitrate tetrahydrate, cobalt and nickel nitrate hexahydrates, respectively. Those salts were mixed with selected nucleating agents to supress supercooling, and then tested under repeating of heating-cooling cycles. Calcium nitrate tetrahydrate showed reversible liquid – solid process with addition of CaO, $Ca(OH)_2$, BaO, $Ba(OH)_2.8H_2O$, graphite and graphene but the supercooling remains too high, and the enthalpy change significantly decreased. In the case of cobalt nitrate hexahydrate, the CaO, $Ba(OH)_2.8H_2O$ and graphite is the most effective nucleating agent in amount of 1 mass%. The supercooling of nickel nitrate hexahydrate was effectively reduced by addition of CaO, $Sr(OH)_2$ and graphite. The cobalt and nickel nitrates were tested with combination of two nucleating agents (1:1). The best results were obtained for composites with addition of 1 mass% of nucleating agent mixture consisting of both graphite and $Ba(OH)_2.8H_2O$ for cobalt nitrate hexahydrate, and CaO with $Mg(OH)_2$ for nickel nitrate hexahydrate.

* pavla.honcova@upce.cz; tel. No. +420466037179

Keywords: Calcium nitrate tetrahydrate; Cobalt nitrate hexahydrate; Nickel nitrate hexahydrate; Dehydration; Phase change materials; DSC; Nucleating agent; Supercooling

Introduction

Inorganic salt hydrates are intensively studied for their ability to store/release quite a high amount of heat during their phase-change, i.e. melting and crystallisation, occurred in low and medium temperature ranges [1-3]. The main advantage of this kind of material is a small volume change associated to solid – liquid phase change, high amount of heat, good thermal conductivity and lower cost. However, there are also disadvantages as an occurrence of supercooling (temperature of melting during charging is higher than temperature of crystallization during discharging), phase separation and corrosion of metal containers/capsules [4-7].

When the phase-change materials (PCMs) are heated above the melting point followed by cooling down, then the crystallization cannot occur. Then the observed supercooling can reach values of order of units or even tens of Kelvin. Thus, the effectivity of charging/discharging process at temperature close to the melting temperature is significantly reduces by supercooling and this undesired effect had to be avoided as was published for several salt hydrates [8-10]. However, the suppression of supercooling needs to be solved mainly if we want the PCM working temperature to be within a narrow range around the melting point. There are several approaches to reduce supercooling, which are predominantly associated with primary heterogeneous nucleation; i.e. nucleation at the surface of foreign bodies such as surface of heat exchanger or container, suspended particles (nucleating agents) or bubbles. [2, 8, 11-13] However, the value of supercooling can be also affected by cooling rate, which is related to the rate of heat transfer from the system. [9, 14]. The addition of seed particles of supercooled material can be used (i.e. secondary nucleation) as well as initiation of crystallization by physical mechanisms as agitation, friction, shock waves or ultrasonic vibration [11, 15]. On the other side, the supercooling may also be an advantage, when supercooled PCM is stable for a long time at ambient temperature and we can initiate discharging process only when needed (as can be charging during the summer time and discharging in winter). In this case, high stability of PCM in supercooled state is the key for practical application [3, 14, 16]. Crystallization and stability in the supercooled state are related to the nucleation process followed by growth of crystals. Thus, understanding of factors and methods to control both these processes is a fundamental to advance thermal energy storage technology. [8, 9, 17].

The congruently melting salt hydrates are preferably tested as phase change materials (PCMs) but also incongruently melted salt hydrates are tested and show reversibility of the process. However, unsuccessful crystallization of colourless salt $Ca(NO_3)_2 \cdot 4H_2O$ (referred as CaNT in following text) cooled below its melting point (42-47 °C [1, 18-25] etc. see Table 1) more than 30 °C [18, 22, 26] was published. Nevertheless, red crystalline cobalt nitrate hexahydrate (reffered as CoNH in following text) with melting point of 55-60 °C [20, 27-29], and green crystalline nickel nitrate hexahydrate (reffered as NiNH in following text) melting at 54-57 °C [20, 27, 28, 30-33,] belong to incongruently melting salts leading to formation of hexahydrate melt/solution and solidification of cobalt nitrate tetrahydrate [34] or nickel nitrate tetrahydrate [35], respectively. Because of decreasing storage efficiency caused by formation of lower hydrated salts and consequently disabling of repeating of heating-cooling cycle the incongruent melting hydrates usually requires testing of pure salt in mixture with stabilizing/nucleating compounds, such in case of $CaCl_2 \cdot 6H_2O$, $CH_3COONa \cdot 3H_2O$ [1, 23].

All three salts belong to group of medium thermal range applicable phase change material. The published melting temperature (T_m), enthalpy of fusion ($\Delta_{fus}H$), specific heat capacity (c_p^T), density in solid state ($\rho_{(s)}^T$) and possible supercooling ($\Delta T = T_m - T_{cr}$) are listed in Table 1. Data summarised in this table declare that in literature can be found several values of T_m and $\Delta_{fus}H$ but there is only little information about crystallization and even less about crystallization behaviour during repeated temperature cycles. [12, 17, 36, 37].

This work contributes to studies of repeated melting-crystallization process of three incongruently melting salt hydrates (CaNT, CoNH and NiNH), tests of nucleating agents with different crystal lattice system to supress supercooling and evaluation of ability and stability of these salts for use in thermal energy storage area. The melting as well as crystallization was evaluated for all tested samples.

Experimental

Calcium nitrate tetrahydrate ($Ca(NO_3)_2 \cdot 4H_2O$) (Penta, 99.0% purity), cobalt nitrate hexahydrate ($Co(NO_3)_2 \cdot 6H_2O$) (Sigma – Aldrich, 99.0% purity) and nickel nitrate hexahydrate ($Ni(NO_3)_2 \cdot 6H_2O$) (Penta, 99.0% purity) were of an analytical reagent grade and stored at room conditions. Their structures were checked by X-ray diffraction analysis performed at 25 °C on diffractometer MiniFlex600 (Rigaku) and the diffraction pattern sheets from the International Centre for Diffraction Data (ICDD) Powder Difraction File (PDF-2) were used. The density of salts hydrates was determined using helium pycnometer Autopycnometer 1320 (Micromeritics) working at laboratory temperature. The heat capacity

was determined using Calvet type calorimeter C80 (Setaram) and the stepwise method [38, 39] with the accuracy of 1 %. Any pre-treatment of the samples (as drying of humidity) was not performed before their characterisation to specify their properties in the form in which they are used for accumulation ability tests.

The thermal properties of salt hydrates were characterised using simultaneous thermogravimeter with differential scanning calorimeter TG-DSC Labsys (Setaram). The sample amount ca. 30 mg in corundum crucible was measured in the temperature range of 25 -300 °C (up to 400 °C only for NiNH), heating rate of 2 K min^{-1} was apply and the argon atmosphere with flow of 50 ml min^{-1} was used. The setting of temperature and the heat flow of equipment was calibrated using pure metals.

Nucleating agent, alone or in the form of a mixture of two of them, were tested to supress supercooling observed in pure CaNT, CoNH or NiNH. Nucleating agents AlO(OH) (Böhmite, >94%, Sasol), BaO (97%, Aldrich), $Ba(OH)_2.8H_2O$ (≥98%, Lachner), $BaCO_3$ (≥99%, Penta), CaO (≥97%, Penta), $Ca(OH)_2$ (≥96%, Lachner), $CaCO_3$ (≥99%, Penta), MgO (≥98%, Penta), $Mg(OH)_2$ (≥99%, Sigma-Aldrich), $MgCO_3$ (basic, 84%, Lachner), $Sr(OH)_2$ (≥94%, Aldrich), $SrCO_3$ (99%, Penta), graphite (98 %, 200 mesh ultrafine, Jinkuancheng Carbon), graphene (98 %, 1-5 layer, Graphene Epoxies) and TiO_2 (RGX, Precheza) were all in analytical purity. The mixtures of salt hydrate with nucleating agent were prepared in solid state by weighting the appropriate amount of components into agate mortar (approximately 0.5 g of the mixture), and mixed for 3 min. All prepared mixtures of CaNT were dry during the mixing but the mixtures prepared using CoNH or NiNH started to be slightly wet during mixing.

Calorimetric measurements were taken using a DSC Pyris 1 (Perkin-Elmer) with an Intracooler 2P. The calorimeter was calibrated using melting temperature of pure metals (Hg, Ga, In, Sn, Pb and Zn) and the enthalpy change was calibrated using the heat of fusion of indium. Three salt hydrates, either pure or as a mixture with other substance, were tested in temperature range from -20 to 80 °C using the heating and cooling rate of 10 K min^{-1} in a closed aluminium crucible in the atmosphere of dry nitrogen with a flow rate of 20 ml min^{-1}. The sample mass was ca. 12 mg. Firstly, the pure salts for determination of supercooling and then their mixture with 1 mass% of each nucleating agent were tested during four heating/cooling cycles (called as fast cycles in following parts). The extrapolation of the onset temperatures was used to determine the melting, T_m, and crystallization, T_{cr}, temperatures (evaluation is similar to that illustrated in Fig. 1 of Ref. [6]). The heat of fusion $\Delta_{fus}H$, and the

heat of crystallization, $\Delta_{cr}H$, were calculated from the area of DSC peaks (if there is any additional effect the enthalpy change was evaluated too as $\Delta_{tr}H$ for heating scan and $\Delta_{tr}H_{(c)}$ for cooling scan). To evaluate the sample ability for thermal energy storage, the average values of T_m, T_{cr}, $\Delta_{fus}H$ and $\Delta_{cr}H$ were calculated without the results for the first cycle for all DSC cycle tests because of the different character of the sample compare to later scans. Separated crystals melts during the first heating and consequently the compact sample is formed during the first cooling, thus, a homogeneous compact sample was formed for the next steps. Based on the high value of enthalpy changes together with the low value of supercooling, ΔT, the promising mixtures were selected as well as combination of effective nucleating agents were suggested. Afterwards, the best compositions were also tested using slow heating/cooling rate of 2 K min^{-1} in four cycles (called as slow cycles in following parts). Subsequently, the compositions of CoNH and NiNH with the 1 mass% of the mixtures of two nucleating agents (both nucleating agents were mixed in ratio 1:1 in solid) were tested using again four fast cycles and the best two compositions for each salt were tested using fifty fast cycles.

Results and discussion

X-ray analysis confirmed that the studied salt hydrates correspond to single crystalline phase as PDF file for CaNT (00-026-1406), CoNH (00-025-1219) and NiNH (00-025-0577). The density of all salt hydrates is solid state were determined as well as heat capacity of CoNH and NiNH. The results are summarised in Table 1 together with literature data. The value of melting temperature, the enthalpy of fusion and the supercooling were determined from the first heating/cooling DSC scans. All experimental values given in Table 1 correspond well to literature data except value of supercooling. Experimental value of ΔT for CaNT is significantly higher than published one and in the case of CoNH and NiNH the value was not found in literature.

Thermogravimetry

The TG/DSC analysis up to 300 °C of all studied salt hydrates was done using samples without any pre-treatment to characterise the samples in the form used for accumulation ability tests. In the case of calcium nitrate tetrahydrate the TG-DSC curve similar to that published by Vollmer and Ayers [40] and Badica et al. [41] was obtained as can be seen in Fig. 1A. The first endothermic effect started at 46 °C corresponds to incongruent melting and formation of liquid solution containing α-$Ca(NO_3)_2{\cdot}2H_2O$ and $Ca(NO_3)_2{\cdot}3H_2O$ [40] with the

enthalpy change of 101 J g^{-1}. The second significant endothermic effect starts at 150 °C and reflect the liquid solution boiling overlapping with decomposition of calcium nitrate hydrates finished at temperature of 220 °C [41] with overall enthalpy change of 350 J g^{-1}. In the temperature range of 66 - 80 °C there is a small endothermic effect also observed by Vollmer and Ayers [40] with the enthalpy change of 6 J g^{-1} which is probably connected with the transformation to di- and trihydrate salts. The mass loss (ca. 31 %) observed in the measured temperature range corresponds to water vaporization, which starts slowly during the melting of CaNT as the first step up to 150 °C followed by other two steps' processes up to 220 °C. Slightly different mechanism was described by Brockner et al [35] using TG data obtained under quasi-isothermal conditions in the temperature range where the dehydration of tetrahydrate into trihydrate is considered followed by formation of $Ca(NO_3)_2 \cdot 2.5H_2O$ and finally $Ca(NO_3)_2$ at 220 °C. The comparison of experimental total mass loss up to 220 °C with the results published by Vollmer and Ayers [40] leads to 4 % of the difference but comparison with data published by Brockner et al [35] leads only to 0.7 % of difference. However, the theoretical mass loss of CaNT dehydration into $Ca(NO_3)_2$ is 30.5 %, thus only 0.5 % corresponds to humidity of CaNT sample used in this study (0.5% is within the experimental error limit).

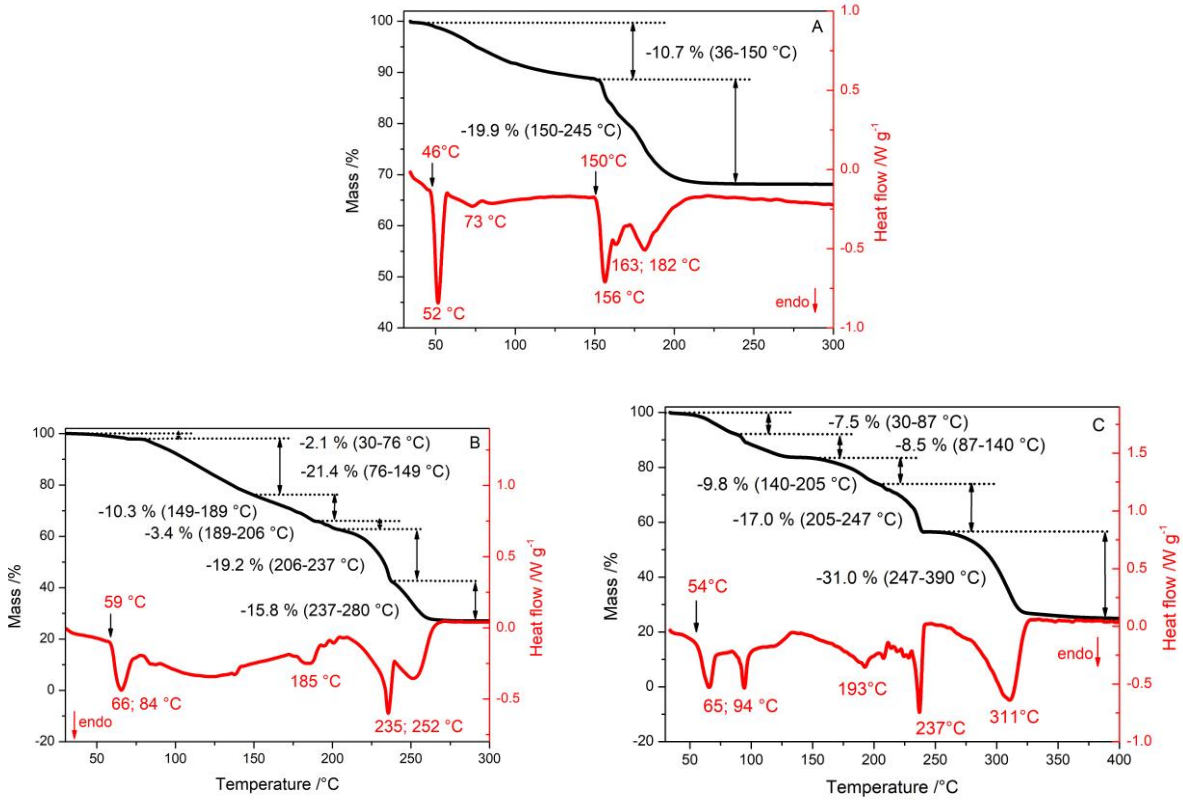

Fig. 1: TG/DSC experimental curves for A) CaNT, B) CoNH and C) NiNH measured in argon atmosphere and heating rate of 2 K min^{-1}

The TG-DSC technique applied to CoNH in the temperature range up to 300 °C shows several overlapping effects as is illustrated in Fig. 1B. This complicated behaviour can be explained when the overlapping peaks can be separated which was done by Ehrhardt et al [34] using quasi-isothermal conditions. They found (heating rate between the quasi-isothermal steps was 0.6 K min^{-1}) that dehydration of CoNH into tetrahydrate starts at temperature about 35 °C that is below the melting temperature. The dehydration process continuously goes through dihydrate into anhydrous cobalt(II) nitrate which should be finished up to 120 °C. Heating of sample to higher temperature caused thermal decomposition and formation of cobalt oxides Co_2O_3 and Co_3O_4 in inert atmosphere [34]. However, the dehydration of dihydrate can be accompanied by formation of cobalt(III) oxonitrate followed by its decomposition into cobalt(II) nitrate (effects observed in the temperature range of ca. 100-130 °C in Ref. [34]). The theoretical mass loss of CoNH dehydration into $Co(NO_3)_2$ is 37.1 %, which is comparable with our total mass loss up to 206 °C (37.2 %). However, concerning the complicated character of dehydration of CoNH and expecting that the humidity of the sample will leave during the first mass loss step we can suppose that the humidity of CoNH sample used in this study is below 2 %. The experimental DSC data reveals several endothermic effects and the temperature corresponding to the maximum of the main peaks is given in Fig. 1B. As can be seen the effects significantly overlapped which caused that there is no clear zero line in the temperature range of 59 – 270 °C. Thus, the area of the peak used to determine the enthalpy change of reaction is only rough estimation (peak baseline follows the line before and after evaluated peak). The first endothermic effect started at 59 °C corresponds to incongruent melting with the enthalpy change of 70 J g^{-1}. Nevertheless, simultaneously the dehydration process started, so the effect in the temperature range of 78-91 °C with the enthalpy change of 6 J g^{-1} and effect in the temperature range of 172 – 193 °C with the enthalpy change of 28 J g^{-1} can be attributed to dehydration. On the other hand, the sharp effect started at 209 °C and overlapped with broader effect finished at 271 °C with overall enthalpy change of 347 J g^{-1} reflecting the formation of cobalt oxides mentioned above.

TG-DSC data of NiNH show complicated behaviour similar to CoNH as can be seen in Fig. 1C but the temperature range of experiment had to be increased to 400 °C. The dehydration of NiNH goes through tetra- and dihydrate. However, Brockner et al [35] showed

(using TG data obtained under quasi-isothermal conditions) that dehydration process does not lead to anhydrous $Ni(NO_3)_2$ but $Ni(NO_3)(OH)_2 \cdot H_2O$ is formed and at higher temperature (ca. 190-250 °C) decomposed to nickel oxides Ni_2O_3, Ni_3O_4 and NiO. The theoretical mass loss of NiNH dehydration into $Ni(NO_3)_2$ is 37.2 %, but it cannot be compared with experimental TG data because the anhydrous form is not formed. Nevertheless, the experimental total mass loss up to 247 °C is 42.8 %. Expecting that the humidity of the sample will leave during the first mass loss step, which is only 1% up to 56 °C, we can suppose that the humidity of NiNH sample used in this study is about 1 %. The DSC scan shows several endothermic peaks but their zero line is more clear comparing to CoNH in Fig. 1B. The first endothermic effect started at 54 °C and corresponds to incongruent melting with enthalpy change of 111 J g^{-1}. The second effect with sharp maximum followed by broad part is at temperature range of 84 – 133 °C with enthalpy change of 116 J g^{-1}. Very broad peak appears in the temperature range of 135 – 212 °C giving the enthalpy change of 146 J g^{-1}.In the range of 212-246 °C another peak appears consisting of several smaller effects. The main sharp effect gives the overall enthalpy change of 166 J g^{-1}. The last endothermic effect in the temperature range of 246-332 °C with enthalpy change of 574 J g^{-1} relates to formation of NiO [35].

Fast DSC measurements of pure salt hydrates

DSC experiments of pure salt hydrates provided the temperature and enthalpy of fusion and verified supercooling. These basic values for the pure salts are listed in Table 1 together with published data.

Table 1 The melting temperature, enthalpy of fusion, specific heat capacity, density in solid state and supercooling of CaNT, CoNH and NiNH. T_m, $\Delta_{fus}H$ a ΔT were determined from our data shown in this work from the first heating-cooling cycle.

Salt	T_m /°C	$\Delta_{fus}H$ /J g^{-1}	c_p^T /J g^{-1} K^{-1}	$\rho_{(s)}^T$ /g ml^{-1}	ΔT /°C	**Ref.**
CaNT	42	140.2	-	-	-	[23]
	42.5	131.7	-	-	-	[18]
	42.6	121.6	-	-	-	[24]
	42.6	140	1.46	-	-	[42]
	42.7	125.8	-	-	-	[20]

	42.7	136.4	-	-	-	[21]
	42.9	144.4	1.43[34]	-	>34	[22]
	44.0	155	1.08[25]	-	-	[25]
	47	142.3	-	-	-	[19]
	47	152.9	-	-	-	[1]
	-	-	1.66[25]	-	-	[43]
	47	153	-	-	65	[13]
	-	-	-	1.820[25]	-	[44]
	44	138	1.478[30]	2.01±0.02[25]	>80	This work
CoNH	55-56	-	-	-	-	[27]
	55.5-57	128-142.9	-	-	-	[20]
	57	-	-	-	-	[28]
	~60	-	-	-	-	[29]
	-	-	1.082	1.883[25]	-	[44]
	-	-	1.56[32]	-	-	[45]
	56	140	1.682[35]	2.04±0.05[27]	14	This work
NiNH	54	-	-	-	-	[30]
	54	-	-	-	-	[33]
	56.7	-	-	-	-	[28]
	56.7	-	-	-	-	[31]
	56.7	168	-	-	-	[20]
	56.7	-	-	2.05	-	[46]
	56.8-57.0	-	-	-	-	[32]
	-	-	1.08	2.050[25]	-	[44]
	-	-	1.98[80]	-	-	[45]
	-	-	1.435	-	-	[43]
	57	165	1.771[35]	2.20±0.04[27]	37	This work

The DSC curves of the four cycles of pure hydrated salts are illustrated in Fig. 2 for CoNH (B) and NiNH (C) but only of the two cycles for CaNT (A). As can be seen if Fig. 2A, no crystallization reflects on following DSC cooling curve when CaNT sample was melted.

Thus, only melting temperature of 43.6 °C was evaluated and the enthalpy of fusion 137.9 J g^{-1} was determined from the first heating scan. From the temperature range tested (cooling was finally done down to -45 °C) we can consider that the supercooling is higher than 80 °C. For CoNH the melting temperature is 56.1 °C and the enthalpy of fusion is 140 J g^{-1} for the first heating scan, for NiNH it is 57.0 °C and 165 J g^{-1}, respectively. In the first cycle, the crystallization starts at 42.6 °C with the enthalpy of crystallization of -130 J g^{-1} for CoNH, and 20.2 °C with -108 J g^{-1} for NiNH. . Repeating of the charging-discharging cycles leads to insignificant change of T_m, T_{cr}, $\Delta_{fus}H$, $\Delta_{cr}H$ but the values for the first cycle are always different comparing to following cycles. The supercooling determined from the first and last cycle is 14 °C and 25 °C for CoNH and 37 °C and 20 °C for NiNH. Hence, ΔT can increase with the number of cycles (Fig. 2B) or decrease (Fig. 2C) but still it is very high for any application in accumulation of thermal energy of pure CoNH and NiNH.

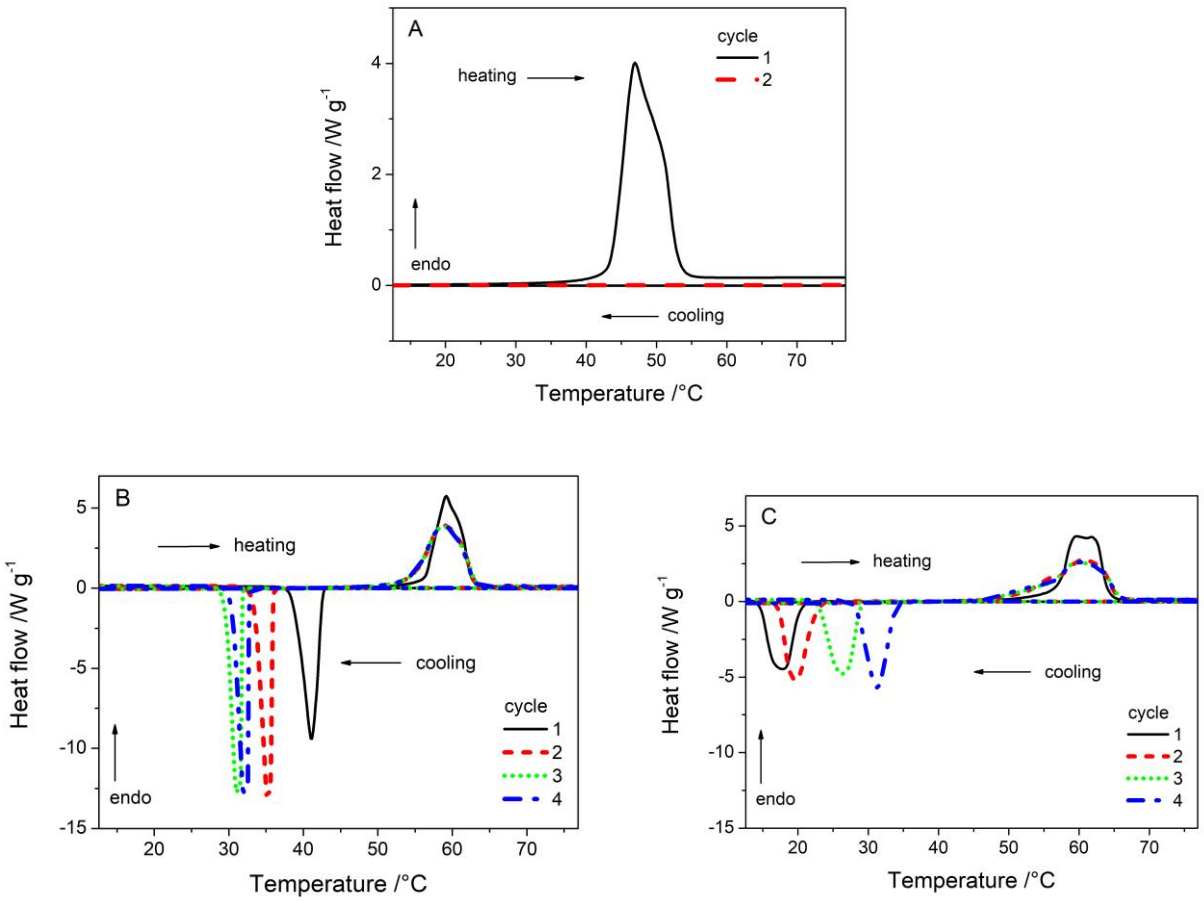

Fig. 2 DSC curves of the first and second cycle for A) CaNT, and up to the fourth cycle for pure: B) CoNH and C) NiNH at heating rate of 10 K min^{-1}.

During the first heating of CoNH we can observe melting peak starting slowly at temperature about 52 °C, then sharp fast increase at about 56 °C following by decreasing part of the peak with shoulder close to the maximum of the peak and end of the peak at temperature about 64 °C. During the subsequent cycles the melting peak is broader and lower, and its increasing part is shifted a bit to lower temperature and the enthalpy change slightly decreases. Moreover, during the repetition of the cycles there is an indication of additional peak appearing in temperature range of 65-70 °C (2B) with the enthalpy change as low as 0.7 J g^{-1}. This effect corresponds to that observed at Fig. 1B and can be connected with formation of tetrahydrate according the thermogravimetry data mentioned above. Occurrence of this peak can negatively influence observed melting and indicates that more thermal cycles of pure CoNH lead to more complex character of endothermic reactions during heating. The crystallization starts during the first cooling scan at temperature about 44 °C but for the following scans it shifts to lower temperature about 35 °C and is narrower (see Fig. 2B) and the enthalpy change is slightly lower comparing to the first cycle. The average supercooling from the second to the fourth cycle is 21.0 ± 2.2 °C and the average values of enthalpy changes during heating ΔH_h and cooling ΔH_c are given in Fig. 6. The values of ΔH_h and ΔH_c are in this work obtained as a sum of any endothermic effects observed at heating (as $\Delta H_h = \Delta_{fus}H + \Delta_{tr}H$ where $\Delta_{tr}H$ corresponds to any transformation) and exothermic effects at cooling scan (as $\Delta H_c = \Delta_{cr}H + \Delta_{tr}H_{(c)}$), respectively.

The melting peak of NiNH is even more complex comparing to CoNH as is illustrated in Fig. 2C. During the first heating scan the narrow melting peak occurs but with plateau instead of sharp maximum. The next scans show small shift of the peak towards lower temperature and partial separation of observed processes with considerable shoulder on the increasing part of DSC peak. The enthalpy change of melting is for the first cycle slightly higher comparing to further cycles. The crystallization during the first cooling scan starts at temperature of 22 °C but with increasing number of cycles is shifted towards higher temperature as is 34 °C for the fourth scan. The enthalpy of crystallization is for the first cycle slightly lower compares to further cycles, which can be attributed to more complex character of process for consecutive cycles. However, this complexity helps to shift crystallization to higher temperature and thus a bit decreases the supercooling. Nevertheless, the changes in T_m and T_{cr} result to the supercooling as high as 25.4 ± 5.9 °C. The average values of enthalpy changes during heating ΔH_h and cooling ΔH_c from 2^{nd} - 4^{th} cycles are given in Fig. 8. The shape of DSC peaks showed complex character of tested salts caused by formation of salts with different degree of

hydration as well as some other effects occurred especially with addition of nucleating agent (which will be discussed later).

DSC measurements of the salt hydrates with 1 mass% of one nucleating agent

The supercooling observed for tested salt hydrates as well as complicated character of melting tried to be suppressed using nucleation agents. Firstly, the only one nucleating agent was mixed with CaNT, CoNH or NiNH and the reversibility and accumulation ability of these mixtures were tested during four fast cycles. The average value of T_m, T_{cr}, ΔH_h and ΔH_c from the second to the fourth cycle was determined and the results are shown in Fig. 3, 6 and 8 for CaNT, CoNH and NiNH. In an effort to obtain the high value of enthalpy changes together with very low supercooling fifteen nucleating agents were mixed with studied nitrate hydrates. The used nucleating agents can be divided into six groups according to crystal structure (The lattice systems and parameters originate from the database of the International Centre for Diffraction Data Powder Diffraction File, PDF-2). The group of cubic system covers BaO, CaO and MgO. The tetragonal system is presented in the rutile crystals. All carbonates and AlO(OH) belong to orthorhombic group. Barium hydroxide octahydrate crystalizes in monoclinic system. The crystal unit of $Ca(OH)_2$ is in trigonal system. The last group forming hexagonal system in $Mg(OH)_2$, graphite and graphene. The isotypic material with tested salt hydrates is the most promising, but non-isotypic material with suitable cell parameters can facilitate epitaxial crystal growth.

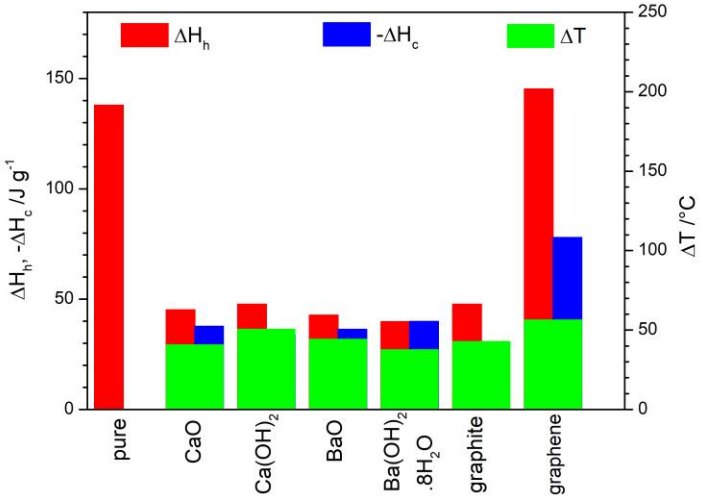

Fig. 3 Enthalpy change on heating (ΔH_h) and sum of enthalpy changes of exothermic effects either on cooling or heating (ΔH_c) and reached supercooling (ΔT) from the first heating scan

of pure CaNT and average values from the 2nd, 3rd and 4th cycles for mixtures of CaNT with addition of 1mass% of nucleating agent.

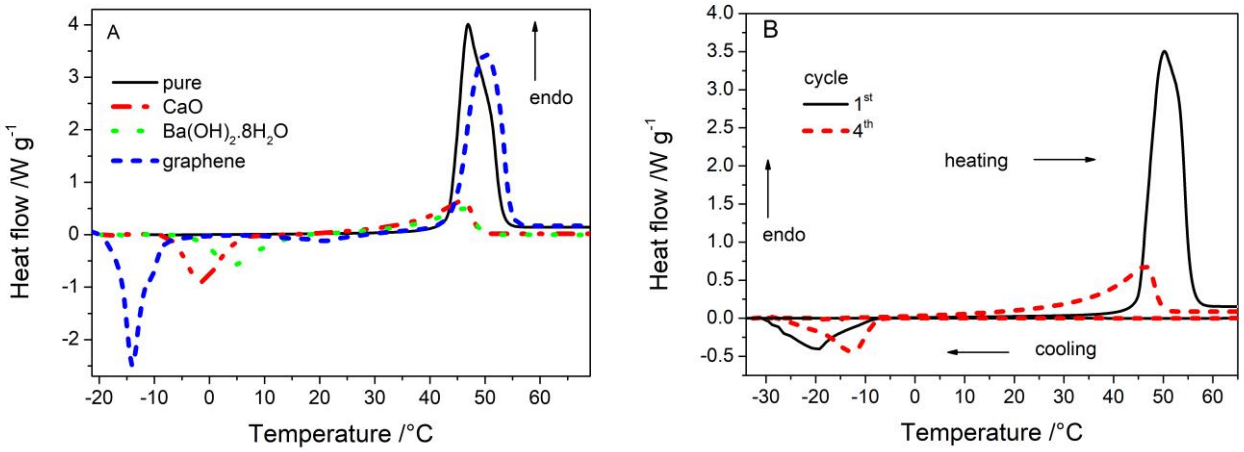

Fig. 4: DSC curves of A) the 1st cycle of CaNT and the 4th cycle of its mixtures with 1 mass% of selected nucleating agent only for heating and B) the 1st and the 4th cycle of mixture with 1 mass% of graphite for heating and cooling.

In the case of CaNT no reversible charging-discharging process was observed similarly to pure CaNT for mixtures with addition of 1 mass% of AlO(OH), $BaCO_3$, $CaCO_3$, MgO, $Mg(OH)_2$, $MgCO_3$, $Sr(OH)_2$, $SrCO_3$ and TiO_2 even if the tested temperature range goes down to -30 °C. However, reversible process was observed for mixtures with addition of 1 mass% of CaO, $Ca(OH)_2$, BaO, $Ba(OH)_2.8H_2O$, graphite and graphene. Unfortunately, the reversibility of (l) – (s) transformation is not optimal as can be seen in Fig. 4 because the exothermic effects do not occur during the cooling but at the beginning of the following heating scan (see Fig. 4A). The only exception is the mixture with graphite (see Fig. 4B) where the exothermic effect occurred during the cooling down below -10 °C. However, the enthalpy of melting is significantly lower when cycles are repeated except the mixture with graphene. The reason is that the sample is not fully crystalline solid. This behaviour was directly observed by testing higher amount of the composite in closed glassy flask in the course of repeated temperature cycles (applied temperature range from -20 to 60 °C using the water baths). The visual evaluation showed that the mixture of solid and liquid phase is formed during heating and consequent cooling. When this mixture stands at room temperature for several hours, it became fully solidified phase identified as CaNT by X-ray diffraction

(formation of any lower hydrate in solid state was not confirmed). The average values of ΔH_h, ΔH_c and ΔT are given in Fig. 3. Unfortunately, these results declare that any of the tested nucleating agents do not successfully supress supercooling which remains in the range of 38 – 57 °C.

The illustration of selected DSC scans of CoNH and its mixtures with 1 mass% of nucleating agents is given in Fig. 5A for heating and Fig. 5B for cooling of the fourth cycle. Concerning the occurrence of the small endothermic peak at temperature above the melting of CoNH, the occurrence of this peak can be found for mixtures with addition of CaO, graphene or BaO. The significant increase of this small effect can be observed for mixtures with addition of TiO_2, graphite and even more for $CaCO_3$ and AlO(OH). The position of the main melting peak in temperature is for all mixtures and pure CoNH almost the same. However, the peak is shifted a bit toward lower temperature for mixture with $SrCO_3$ and on the contrary is shifted toward higher temperature for mixture with MgO, $Mg(OH)_2$, $BaCO_3$ and $Ca(OH)_2$. The height of the main melting peak is even higher for mixture with $CaCO_3$ than for pure CoNH. For other mixtures the main melting peak is lower and its maximum is broader comparing to pure CoNH. The melting peak is the lowest for the mixture with $SrCO_3$, $Mg(OH)_2$, MgO, $Ca(OH)_2$ and $Sr(OH)_2$. During the cooling of pure CoNH or its mixtures with nucleating agent the crystallization was observed. The crystallization peak of pure CoNH is narrow and sharp as can be seen in Fig. 5B. The similar shape was observed for mixture with graphene, AlO(OH) and $CaCO_3$. The crystallization peak for mixtures with other nucleating agents shows lower peak but still narrow. However, the lower crystallization peak and broad maximum was observed for the mixtures with MgO, TiO_2, $Ca(OH)_2$, $Mg(OH)_2$ but in that case the peaks were simultaneously shifted to higher temperature (see Fig. 5B).

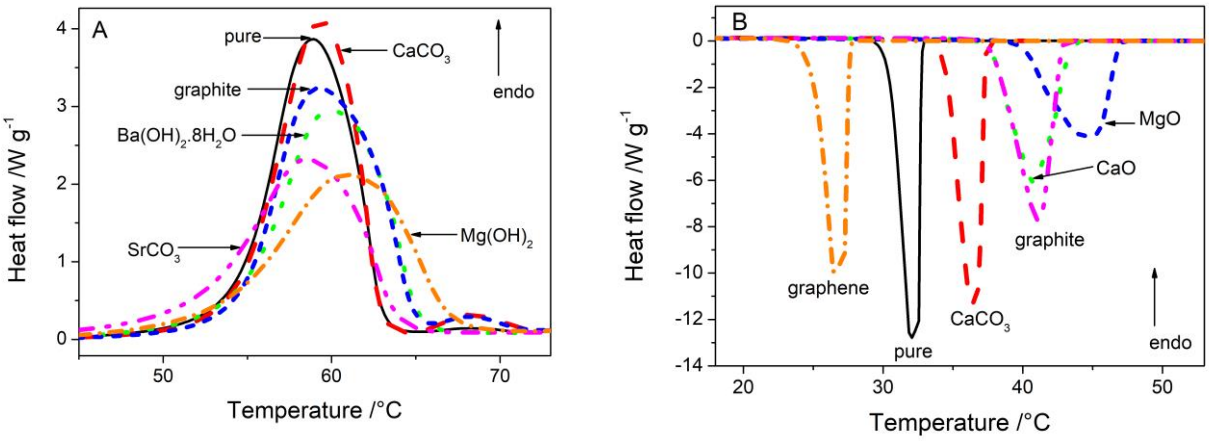

Fig. 5: DSC scans of the 4th cycle for CoNH and its mixtures with 1 mass% of selected nucleating agent for A) heating and B) cooling.

Taking in mind the shape of the melting and crystallization peaks as well as the values of the enthalpy changes and supercooling (Fig. 6), the best accumulation ability is provided by mixtures of CoNH with 1 mass% of non-isotypic nucleators as CaO and graphite. The last auspicious agent is isotypic $Ba(OH)_2.8H_2O$. These promising mixtures were further tested by the slow four cycles using the heating/cooling rate of 2 K min^{-1}. This slow rate is closer to real conditions comparing to fast DSC cycles using the rate as high as 10 K min^{-1}. The comparison of characteristic parameters for fast and slow cycles is given in Table 2. The melting temperature is not significantly affected by the change of heating/cooling rate and T_{cr} changing only a bit comparing to the rate of 10 K min^{-1}. Enthalpy change of heating is for lower heating rate higher comparing to higher rate except mixture with CaO. The supercooling is lower with lower heating rate only for mixture with CaO. The other mixtures provide ΔT values similar for both tested rates, excluding use of graphite, which caused increase of the supercooling.

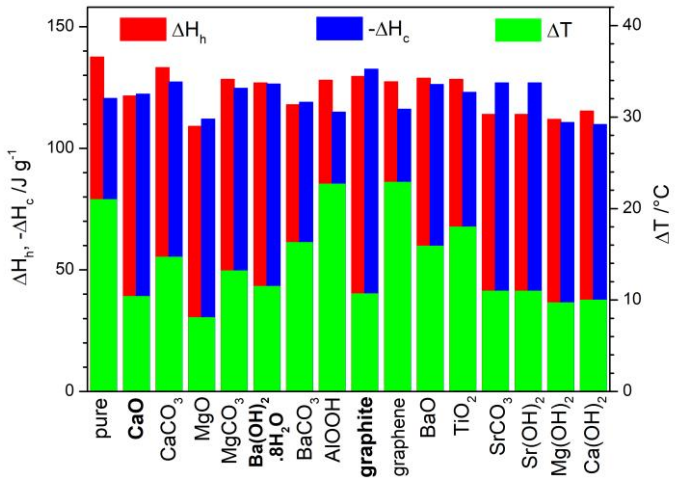

Fig. 6: Enthalpy change on heating, ΔH_h, and cooling, ΔH_c, and reached supercooling, ΔT, average from the 2nd, 3rd and 4th cycles of pure CoNH and mixtures of CoNH with addition of 1mass% of nucleating agent. The legend in bold emphasizes the best mixtures.

Table 2 The value of melting temperature (T_m), enthalpy change during heating (ΔH_h), temperature of crystallization (T_{cr}), enthalpy change during cooling (ΔH_c) and supercooling (ΔT) of pure CoNH and CoNH with addition of 1 mass% of nucleating

agent. An average values were calculated from the 2nd- 4th cycles of fast as well as slow cycles.

Nucleating agent	rate /K min^{-1}	T_m /°C	ΔH_h /J g^{-1}	T_{cr} /°C	ΔH_c /J g^{-1}	ΔT /°C
none	10	54.5 ± 0.1	137.5 ± 0.9	33.5 ± 2.2	-120.6 ± 3.0	21.0 ± 2.2
	2	55.7 ± 0.1	155.6 ± 1.2	33.4 ± 3.3	-125.3 ± 1.9	22.3 ± 2.5
CaO	10	54.1 ± 0.1	121.5 ± 0.3	43.7 ± 0.3	-122.3 ± 0.2	10.4 ± 0.3
	2	53.1 ± 0.1	111.1 ± 4.5	45.0 ± 0.5	-117.8 ± 0.3	8.1 ± 0.5
Ba(OH)2.	10	54.5 ± 0.1	126.9 ± 1.0	43.1 ± 0.6	-126.4 ± 0.3	11.5 ± 0.6
8H2O	2	55.1 ± 0.1	149.3 ± 1.4	44.0 ± 3.3	-128.1 ± 1.2	11.1 ± 3.4
graphite	10	54.7 ± 0.1	129.6 ± 0.8	44.0 ± 0.9	-132.5 ± 0.3	10.7 ± 0.9
	2	54.6 ± 0.1	155.1 ± 5.9	41.6 ± 4.5	-133.4 ± 2.1	13.0 ± 4.5

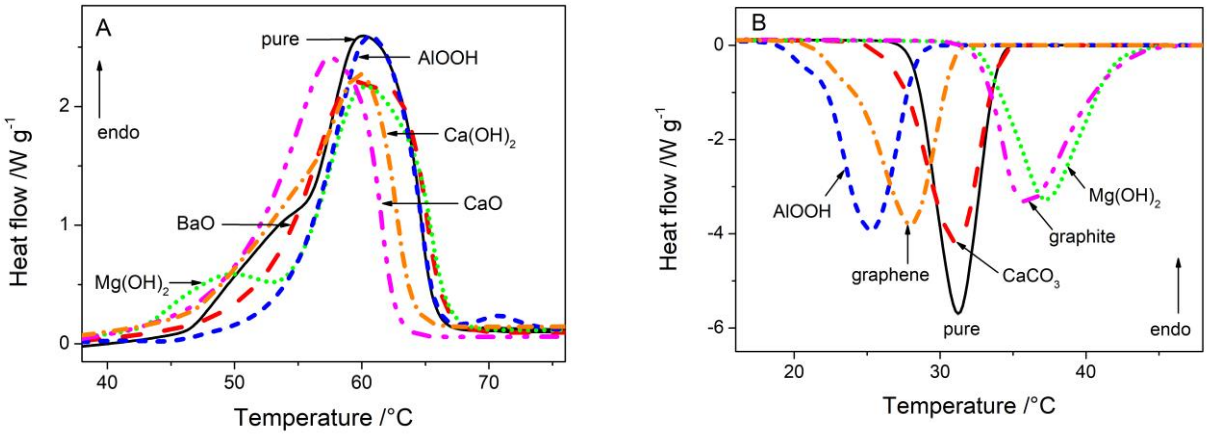

Fig. 7 DSC scans of the 4th cycle for NiNH and its mixtures with 1 mass% of selected nucleating agent for A) heating and B) cooling.

As was mentioned above and illustrated in Fig. 2C, the heating scan of NiNH gives complex endothermic effect connected with melting of NiNH and probably also with the formation of lower salt hydrate (in agreement with the result of thermogravimetry results shown in Fig.

1C). The selected DSC scans of NiNH and its mixtures with 1 mass% of nucleating agents are given in Fig. 7A for heating and Fig. 7B for cooling of the fourth cycle. At the heating, the noticeable shoulder on the increasing part of the peak similar to that observed for the pure NiNH was also obtained for mixtures with majority of tested nucleating agents. However, the mixture with addition of BaO or $Sr(CO_3)_2$ showed plateau instead of maximum of the peak and no indication of shoulder on the effect. The simple main peak was observed for mixture with AlO(OH) with the additional small endothermic affect occurred at higher temperature similarly as was observed for the same nucleating agent mixed with CoNH. Probably part of the melted acidic nitrate can react with alkaline Böhmite. The temperature corresponding to the maximum of endothermic peak on DSC heating scans is for all tested nucleating agents almost the same within the 5°C range as is seen in Fig. 7A. The height of the main endothermic peak is similar to that of pure NiNH for all tested nucleating agents. Only mixture with graphene provided a bit higher peak and even higher show the mixture with $BaCO_3$ or TiO_2. The illustration of exothermic effect of crystallization obtained during the cooling of the samples is given in Fig. 7B. Pure NiNH shows single sharp peak and similar behaviour was observed for mixture with majority of tested nucleating agents. The shoulder on decreasing part of the peak was observed for mixture with AlO(OH), graphene, TiO_2 and $SrCO_3$. Significantly broader crystallization peak showed mixture with $Mg(OH)_2$ and even indication of shoulder on increasing part of the peak was observed for mixture with graphite. The temperature corresponding to the beginning of crystallization peak as well as maximum of the peak differs depending on nucleation agent added to NiNH and change within the range of 15 °C (see Fig. 7B).

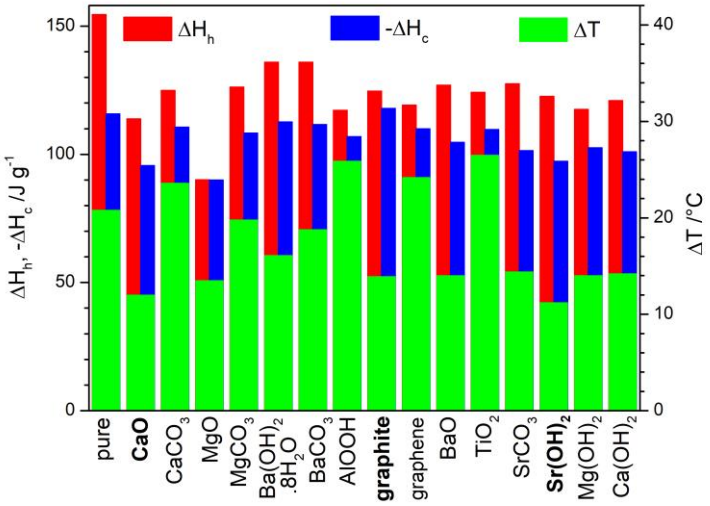

Fig. 8: Enthalpy change on heating, ΔH_h, and cooling, ΔH_c, and reached supercooling, ΔT, average from the 2nd, 3rd and 4th cycles of pure NiNH and mixtures of NiNH with addition of 1 mass% of nucleating agent. The legend in bold emphasizes the best mixtures.

Taking into account the shape of the melting and crystallization peaks as well as the values of the enthalpy changes together with supercooling (Fig. 8), the best accumulation ability shows mixtures of NiNH with 1 mass% of epitaxial nucleating materials (PDF-2 database) including CaO (cubic crystals with lattice parameter a = 4.8 Å), graphite (hexagonal crystals with a, b = 2.5 Å and c = 9.1 Å) or $Sr(OH)_2$ (orthorhombic, a = 6.1, b = 9.9 Å and c = 3.9 Å). These promising mixtures were more thoroughly tested in the slow four cycles using the heating/cooling rate of 2 K min^{-1}. The comparison of characteristic parameters for fast and slow cycles is given in Table 3. The application of lower rate caused that the melting temperature shifts of ca. 2 °C to lower temperature and T_{cr} increased a bit. Thus, the supercooling decreases for lower rate for pure NiNH and all three tested nucleating agents and the minimum value was obtained for mixture with addition of graphite. The enthalpy change of heating is slightly lower for lower rate for NiNH and addition of CaO whereas is a bit higher for addition of $Sr(OH)_2$ and graphite. The enthalpy change of cooling is for lower rate a bit lower for mixture with CaO, but other samples showed higher value in comparison with rate of 10 K min^{-1}.

Table 3. The value of melting temperature (T_m), enthalpy change during heating (ΔH_h), temperature of crystallization (T_{cr}), enthalpy change during cooling (ΔH_c) and supercooling (ΔT) of pure NiNH and NiNH with addition of 1 mass% of nucleating agent. An average values were calculated from the 2nd- 4th cycles of fast as well as slow cycles.

Nucleating agent	**rate /K min^{-1}**	T_m **/°C**	ΔH_h **/J g^{-1}**	T_{cr} **/°C**	ΔH_c **/J g^{-1}**	ΔT **/°C**
none	10	54.0 ± 0.2	154.5 ± 2.2	33.2 ± 4.7	-115.8 ± 2.4	20.8 ± 4.6
	2	52.5 ± 0.1	149.2 ± 1.7	37.0 ± 1.6	-118.8 ± 0.6	15.5 ± 1.6
CaO	10	50.4 ± 0.4	113.8 ± 1.7	38.4 ± 0.3	-95.6 ± 0.5	12.0 ± 0.7
	2	48.6 ± 0.2	99.7 ± 5.0	40.7 ± 0.2	-90.3 ± 0.4	8.0 ± 0.3
$Sr(OH)_2$	10	55.0 ± 0.1	122.6 ± 1.1	44.1 ± 1.1	-97.3 ± 1.0	11.2 ± 1.0
	2	52.7 ± 1.2	129.5 ± 3.4	42.2 ± 0.4	-111.2 ± 0.9	10.5 ± 1.6
graphite	10	54.7 ± 0.1	124.7 ± 0.6	40.7 ± 0.7	-117.9 ± 0.3	13.9 ± 0.8

2	52.5 ± 0.1	148.7 ± 1.1	46.7 ± 2.4	-116.0 ± 0.3	5.8 ± 2.3

DSC measurements of the salt hydrates with 1 mass% of mixture of two nucleating agents

The supercooling observed in composites formed by addition of one nucleating agent is about 10 °C and still it is too high for practical applications. That is why the mixtures consisting of two promising nucleating agents were tested. The results for composites with CoNH are given in Fig. 9 and for NiNH in Fig. 10. In the case of CoNH based samples, the addition of nucleating agents' mixture does not significantly reduce the enthalpy change for heating or cooling compared to pure CoNH, but effectively reduce the supercooling. The best results with ΔT equal to 6 °C and 5 °C were obtained for mixture with addition of graphite – MgO and graphite – $Ba(OH)_2.8H_2O$, respectively.

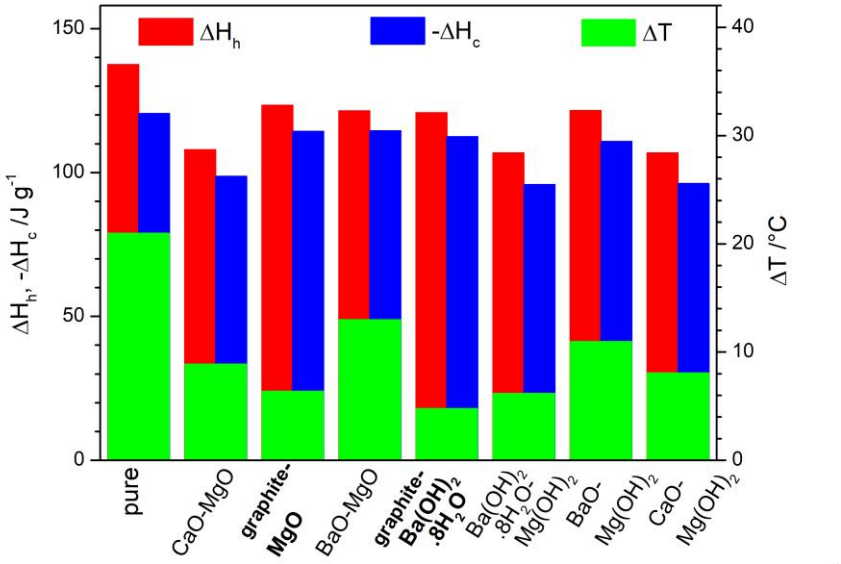

Fig. 9 Enthalpy change on heating, ΔH_h, and cooling, ΔH_c, and reached supercooling, ΔT, average from the 2nd, 3rd and 4th cycles of pure CoNH and mixtures of CoNH with addition of 1 mass% of mixture of two nucleating agents. The legend in bold emphasizes the best mixtures.

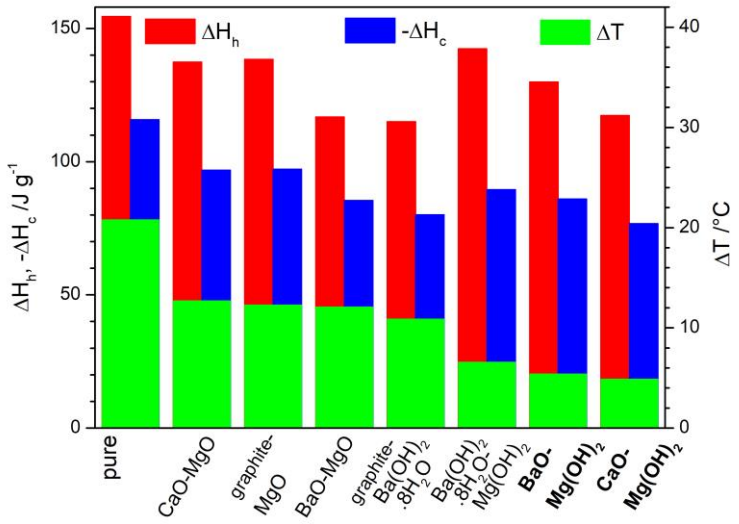

Fig. 10: Enthalpy change on heating, ΔH_h, and cooling, ΔH_c, and reached supercooling, ΔT, average from the 2nd, 3rd and 4th cycles of pure NiNH and mixtures of NiNH with addition of 1 mass% of mixture of two nucleating agents. The legend in bold emphasizes the best mixtures.

In the case of NiNH based samples (Fig. 10), the addition of nucleating agents' mixture slightly reduces the enthalpy change for heating and mainly for cooling compared to pure NiNH. However, in all cases the addition of nucleating agents' mixture effectively reduce the supercooling which is only 5 °C for BaO-$Mg(OH)_2$ and CaO-$Mg(OH)_2$ mixtures and 7 °C for mixture with $Ba(OH)_2.8H_2O$ -$Mg(OH)_2$.

Nevertheless, the practical application of PCM requires material that is stable within a large number of cycles. That is why the best compositions given in bold in Fig. 9 and 10 were tested using fifty fast cycles and the results are summarised in Table 4. In the case of CoNH and its mixture with graphite – MgO, the low supercooling was kept until the tenth cycle, but then increased to 10 °C and this value remained until the fiftieth cycle. The increase of supercooling is caused by shift of crystallization towards lower temperature. Similarly, the mixture of CoNH with addition of graphite – $Ba(OH)_2.8H_2O$ behaved, but the increase of supercooling occurred around the fifteenth cycle and its value remained lower. Therefore, this is the best composition with the lowest supercooling value for CoNH. A similar increase in supercooling with a larger number of cycles was observed for NiNH, where supercooling increased since the tenth cycle for mixture with BaO-$Mg(OH)_2$, whereas with admixture of CaO-$Mg(OH)_2$ the low value is maintained until the fortieth cycle and even then the value is

not very high. Thus, the mixture of NiNH with CaO-$Mg(OH)_2$ gives the best results stable within the fifty cycles.

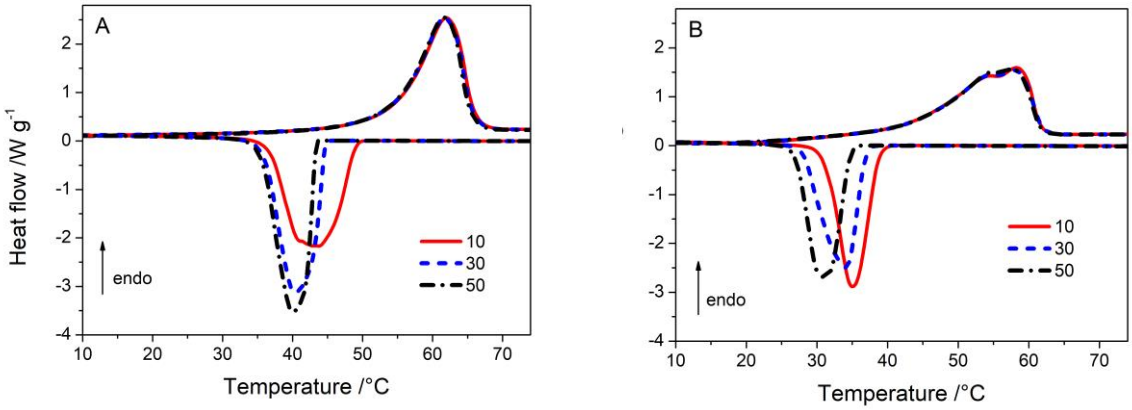

Fig. 11: DSC curves for the tenth, thirtieth and fiftieth cycle for mixture of A) CoNH with 1 mass% of graphite-$Ba(OH)_2 \cdot 8\ H_2O$ and B) NiNH with 1 mass% of CaO-$Mg(OH)_2$.

Table 4. The value of melting temperature (T_m), enthalpy change during heating (ΔH_h), temperature of crystallization (T_{cr}), enthalpy change during cooling (ΔH_c) and supercooling (ΔT) of CoNH and NiNH with addition of 1 mass% of mixture of two nucleating agents. An average values were calculated from the 2^{nd}- 50^{th} cycles of fast cycles.

Composition	T_m /°C	ΔH_h /J g^{-1}	T_{cr} /°C	ΔH_c /J g^{-1}	ΔT /°C
CoNH + 0.5 % graphite + 0.5 % MgO	54.5 ± 0.2	120.9 ± 2.2	44.3 ± 2.5	-113.4 ± 0.6	10.2 ± 2.7
CoNH + 0.5 % graphite + 0.5 % $Ba(OH)_2.8H_2O$	54.3 ± 0.2	120.5 ± 1.5	46.5 ± 2.7	-111.9 ± 0.7	7.9 ± 2.5
NiNH + 0.5 % BaO + 0.5 % $Mg(OH)_2$	50.0 ± 0.5	116.5 ± 1.1	37.1 ± 3.6	-89.6 ± 0.4	12.9 ± 3.2
NiNH + 0.5 % CaO + 0.5 % $Mg(OH)_2$	42.7 ± 0.5	108.7 ± 1.2	37.9 ± 1.5	-82.2 ± 0.3	4.8 ± 1.9

Conclusion

Pure CaNT under heating showed melting at 44 °C and the enthalpy change of fusion is 138 J g^{-1}. During cooling, no reversible (l) – (s) process was observed in the case of CaNT so we can consider that the supercooling is higher than 80 °C. Addition of nucleating agent to CaNT in some cases caused reversibility in (l) – (s) process, but the partial crystallization started

only at the beginning of the heating scan and then consequent melting gave only small enthalpy of fusion. Nevertheless, the addition of nucleating agent into CaNT in some cases reduced the supercooling, but only to 50 °C. Pure CoNH and NiNH under heating showed melting at 56 °C with enthalpy change of 140 J g^{-1} and 57 °C and 165 J g^{-1}, respectively. During the cooling of CoNH and NiNH the crystallization temperature is 43 °C with the enthalpy change of -130 J g^{-1} and 20 °C with -108 J g^{-1}, respectively. Addition of tested nucleating agents into CoNH and NiNH led to decreasing of supercooling except for AlO(OH), graphene, TiO_2 and $CaCO_3$. However, addition of one nucleating agent into CoNH led to supressing supercooling to 8 °C for MgO and 10 °C for CaO. On the other hand, the addition of one nucleating agent was not so effective for NiNH samples where the lowest supercooling was 11 °C for $Sr(OH)_2$ and 12 °C for CaO. Finally, CoNH and NiNH in mixture with two nucleating agents provided the supercooling less than 5 °C for composites of CoNH + 0.5 mass% of graphite + 0.5 mass% of $Ba(OH)_2.8H_2O$, and NiNH + 0.5 mass% of CaO + 0.5 mass% of $Mg(OH)_2$. These two mixtures are also the best stable compositions of longer testing over fifty cycles.

Acknowledgement

This work has been supported by IGA University of Pardubice under the research project SGS_2019_004. The authors acknowledge the assistance provided by the project Pro-NanoEnviCz (Reg. No. CZ.02.1.01/0.0/0.0/16_013/0001821) supported by the Ministry of Education, Youth and Sports of the Czech Republic and the European Union - European Structural and Investments Funds in the frame of Operational Programme Research Development and Education.

References

1. Sharma A, Tyagi VV, Chen CR, Buddhi D. Review on thermal energy storage with phase change materials. Renew Sustain. Energy Rev. 2009;13:318–45.
2. Mohamed SA, Al-Sulaiman FA, Ibrahim NI, Zahir MdH, Al-Ahmed A, Saidur R, Yilbas BS, Sahin AZ. A review on current status and challenges of inorganic phase change materials for thermal energy storage systems. Renew Sustain Energy Rev. 2017;70;1072-89.
3. Zalba B, Marín JM, Cabeza LF, Mehling H. Review on thermal energy storage with phase change: materials, heat transfer analysis and applications. Appl Thermal Eng. 2003;23;251-83.
4. Calabrese L, Brancato V, Paolomba V, Proverbio E. An experimental study on the corrosion sensitivity of metal alloys for usage in PCM thermal energy storage. Renew Energy 2019;138;1018-27.

5. Morano P, Miró L, Solé A, Barreneche C, Solé S, Martorell I, Cabeza LF. Corrosion of metal and metal alloy containers in contact with phase change materials (PCM) for potential heating and cooling applications. Appl Energy 2014;125;238-45.
6. Honcova P, Pilar R, Danielik V, Soska P, Sadovska G, Honc D. Suppressing supercooling in magnesium nitrate hexahydrate and evaluating corrosion of aluminium alloy container for latent heat storage application. J Therm Anal Cal. 2017;129:1573-81.
7. Danielik V, Šoška P, Felgerová K, Zemanová M. The corrosion of carbon steel in nitrate hydrates used as phase change materials. Mater Corros. 2017;68;416-22.
8. Farid MM, Khudhair AM, Razack SAK, Al-Hallaj S. A review on phase change energy storage: materials and applications. En Conv Manag. 2004;45;1597-1615.
9. Safari A, Saidur R, Sulaiman FA, Xu Y, Dong J. A review on supercooling of Phase Change Materials in thermal energy storage systems. Renew Sustain Energy Rev. 2017;70;905-19.
10. Li G, Zhang B, Li X, Zhou Y, Sun Q, Yun Q. The preparation, characterisation and modification of a new phase change material: $CaCl_2 \cdot 6H_2O$- $MgCl_2 \cdot 6H_2O$ eutectic hydrate salt. Sol Energy Mater Sol Cells 2014;126;51-5.
11. Mullin JW. Crystallization. Elsevier, Butterworth-Heinemann, 2001.
12. Khan Z, Khan Z, Ghafoor A. A review of performance enhancement of PCM based latent heat storage system within the context of materials, thermal stability and compatibility. En Conv Manag. 2016;115;132-58.
13. Beaupere N, Soupremanien U, Zalewski L. Nucleation triggering mathods is supercooled phase change materials. Thermochim Acta 2018;670;184-201.
14. Development of a test standard for PCM and TCM characterisation. Part 1: Characterisation of phase change materials. Technical report of IEA Solar Heating and Cooling/Energy Conservation through Energy starage programme – Task 42/Annex 24: Compact thermal energy storage: Material development for system integration. 2011.
15. Awad A, Navarro H, Ding Y, Wen D. Thermal-physical properties of nanoparticle-seeded nitrate molten salts. Renew Energy 2018;120;275-88.
16. Dannemand M, Schultz JM, Johansen JB, Furbo S. Long term thermal energy storage with stable supercooled sodium acetate trihydrate. Appl Therm Eng. 2015;91;671-78.
17. Lane GA. Phase change materials for energy storage nucleation to prevent supercooling. Sol Energy Mater Sol Cells 1992;27;135-60.
18. Angell CA, Tucker JC. Heat capacities and fusion entropies of the tetrahydrates of calcium nitrate, cadmium nitrate, and magnesium acetate. Concordance of calorimetric and relaxational ‘‘ideal’’ glass transition temperatures. J Phys Chem.1974;78:278–81.
19. Lorsch GH, Kauffman KW, Dentons JC. Thermal energy storage for solar heating and off-peak air conditioning. Energy Convers. 1975;15:1–8.
20. Guion J, Sauzade JD, Laügt M. Critical examination and experimental determination of melting enthalpies and entropies of salt hydrates. Thermochim Acta 1983;67:167-79.
21. Naumann R, Emons HH. Results of thermal analysis for investigation of salt hydrates as latent heat-storage materials. J Thermal Anal. 1989;35:1009–31.
22. Xu Y, Hepler GL. Calorimetric investigations of crystalline, molten, and supercooled Ca(NO3)2_4H2O and of concentrated Ca(NO3)2 (aq). J Chem Thermodyn. 1993;25:91–7.
23. Voigt W, Zeng D. Solid-liquid equilibria in mixtures of molten salt hydrates for the design of heat storage materials. Pure Appl Chem. 2002;74:1909–20.
24. Nikolova D, Maneva M. Thermal investigations of nitrate-hydrates and deuterates of Ca(2+), Cd(2+) and Mg(2+). J Therm Anal. 1995;44:869–75.

25. Sádovská G, Honcová P, Pilar R, Oravová L, Honc D. Calorimetric study of calcium nitrate tetrahydrate and magnesium nitrate hexahydrate. J Therm Anal Calorim. 2016;124:539–46.
26. Proceeding Termoanalyticky seminar TAS 2015, University of Pardubice, ISBN 978-80-7395-888-6, p. 29-34.
27. *Knovel Critical Tables (2nd Edition).* (Table Basic Physical Properties of Chemical Compounds). Knovel. Retrieved from https://app.knovel.com/hotlink/toc/id:kpKCTE000X/knovel-critical-tables/knovel-critical-tables
28. Riesenfeld EH, Milchsack C. Versuch einer Bestimmung des Hydratationsgrades von Salzen in koncentrierten Lösungen. Z Anorg Chem. 1914;85:401-29.
29. Mansour SAA. Spectrothermal studies on the decomposition course of cobalt oxysalts. Part II. Cobalt nitrate hexahydrate. Mat Chem Phys. 1994;36;317-23.
30. Paulik F, Paulik J, Arnold M. Investigation of the phase diagram for the system $Ni(NO_3)_2$ – H_2O and examination of the decomposition of $Ni(NO_3)_2 \cdot 6H_2O$. Thermochim Acta 1987;121:137-49.
31. Lohrengel MM, Klüppel I, Rosenkranz C, Bettermann H, Schultze JW. Microscopic investigations of electrochemical machining of Fe in $NaNO_3$. Electrochim Acta 2003;48;3203-11.
32. Marcus Y, Minevich A, Ben-Dor L. Solid-liquid equilibrium diagrams of common ion binary salt hydrate mixtures involving nitrates and chlorides of magnesium, cobalt, nickel, manganese, and iron(III). Thermochim Acta 2005;432:23-9.
33. Metz R, Machado C, Tenu R, Elkhatib M, Letoffe JM, Delalu H. Possible evidence of the nickel nitrate salt $Ni(NO_3)_2.5.5H_2O$. J Phys IV France 2004;113;139-42.
34. Ehrhardt C, Gjikaj M, Brockner W. Thermal decomposition of cobalt nitrato compounds: Preparation of anhydrous cobalt(II) nitrate and its characterization by Infrared and Raman spectra. Thermochim Acta 2005;432;36-40.
35. Brockner W, Ehrhardt C, Gjikaj M. Thermal decomposition of nickel nitrate hexahydrate, $Ni(NO_3)_2 \cdot 6H_2O$, in comparison to $Co(NO_3)_2 \cdot 6H_2O$ and $Ca(NO_3)_2 \cdot 4H_2O$. Thermochim Acta 2007;456;64-8.
36. Alva G, Liu L, Huang X, Fang G. Thermal energy storage materials and systems for solar energy applications. Renew Sustain Energy Rev. 2017;68;693-706.
37. Liu D, Zhu J. Kinetics influence of operation conditions on crystal growth of calcium nitrate tetrahydrate in a circulating fluidized bed. Iranian J Chem Chem Eng. 2018;37;67-73.
38. Application note M149-v1, Setaram.
39. Mraw SC, Naas DF. Measurement of accurate heat-capacities by differential scanning calorimetry Comparison of d.s.c. results on pyrite (100 to 800 K) with literature values from precision adiabatic calorimetry. J Chem Termodyn. 1979;11;567-84.
40. Vollmer N, Ayers R. Decomposition combustion synthesis of calcium phosphate powders for bone tissues engineering. Int J Self-Prop High-temp Synth. 2012;21;189-201.
41. Badica P, Aldica G, Crisan A. Decomposition of Ca:Cu = 1:1 nitrate powder: thermal analysis and structural studies. J Mater Sci. 2002;37;585-94.
42. Telkes M. Thermal energy storage in salt hydrates. Solar Energy Materials 1980;2;381-93.
43. Zhdanov VM, Shamova VA, Drakin SI. Heat capacity of crystal hydrates of magnesium, aluminum, calcium, nickel, and lanthanum nitrates and copper sulfate pentahydrate. Deposited Doc VINITI. 1976;2874–76:1–10.
44. Yaws CL (2012; 2013; 2014). *Yaws' Critical Property Data for Chemical Engineers and Chemists.* Knovel. Retrieved from

https://app.knovel.com/hotlink/toc/id:kpYCPDCECD/yaws-critical-property/yaws-critical-property
45. ICT – *International Critical Tables of Numerical Data, Physics, Chemistry and Technology* (1st Electronic Edition). Washburn EW, Publisher Knovel, Copyright Date 1926 - 1930;2003, ISBN 978-1-59124-491-2.
46. Washburn EW (1926 - 1930;2003). *International Critical Tables of Numerical Data, Physics, Chemistry and Technology (1st Electronic Edition).* Knovel. Retrieved from https://app.knovel.com/hotlink/toc/id:kpICTNDPC4/international-critical/international-critical